MATERIALS SCIENCE

Transient exciton-polariton dynamics in WSe_2 by ultrafast near-field imaging

M. Mrejen[1,2], L. Yadgarov[1], A. Levanon[1], H. Suchowski[1,2]*

Van der Waals (vdW) materials offer an exciting platform for strong light-matter interaction enabled by their polaritonic modes and the associated deep subwavelength light confinement. Semiconductor vdW materials such as WSe_2 are of particular interest for photonic and quantum integrated technologies because they sustain visible–near-infrared (VIS-NIR) exciton-polariton (EP) modes at room temperature. Here, we develop a unique spatiotemporal imaging technique at the femtosecond-nanometric scale and observe the EP dynamics in WSe_2 waveguides. Our method, based on a novel ultrafast broadband intrapulse pump-probe near-field imaging, allows direct visualization of EP formation and propagation in WSe_2 showing, at room temperature, ultraslow EP with a group velocity of $v_g \sim 0.017c$. Our imaging method paves the way for in situ ultrafast coherent control and extreme spatiotemporal imaging of condensed matter.

INTRODUCTION

Van der Waals (vdW) materials offer a malleable playground for a wide range of electronic and optical properties in nanoscale devices. Light-matter quasiparticles (polaritons) are central to these capabilities (*1*–*3*) and, recently, advanced subdiffraction imaging techniques have provided valuable insights into their coupling mechanism (*4*–*8*). However, most of these studies focused on the steady state of these polaritons, leaving their subpicosecond spatiotemporal dynamics in the visible–near-infrared (VIS-NIR) spectral region unexplored. Simultaneously resolving these dynamics at the nanometric and femtosecond scale is crucial for the understanding and development of devices where the nanoscale dimensions directly affect the ultrafast transient of these hybrid light-matter modes. Here, we develop a novel ultrafast pump-probe near-field imaging method and report the ultrafast and deep subwavelength direct visualization of exciton-polariton (EP) formation and propagation in WSe_2 waveguides. We directly observe, at room temperature, an ultraslow EP wave packet with a group velocity of $v_g \sim 0.017c$. While these findings point toward vdW material–based slow light applications such as photonic memory, enhanced optical nonlinearity, and sensing, our imaging method paves the way for in situ ultrafast coherent control and extreme spatiotemporal imaging of condensed matter systems.

In recent years, vdW materials, such as graphene and hexagonal boron nitride, have come forth as a new material platform supporting a plethora of coupled modes of light and crystal polarization, also known as polaritons, such as plasmon polariton and phonon polariton, offering unique properties (*9*–*13*). On the other hand, transition metal dichalcogenides (TMDs) with chemical formula MX_2 (M = Mo and W; X = S, Se, and Te) are vdW semiconductors with sizeable bandgaps in the VIS-NIR spectral region and with tightly bound excitons (*3*, *14*). These excitons can couple with photons, provided they have the means to bridge the momentum gap, and form EPs (*1*, *2*), which have been observed in the VIS-NIR spectral region at ambient conditions. Far-field optical studies of TMDs embedded in microcavities have captured the spectroscopic signatures of strongly coupled cavity EPs (*15*, *16*). More recently, the light-exciton coupling has been demonstrated to be achievable via waveguide modes in subwavelength vdW material structures (*4*–*6*). The real-space characteristics (for example, propagation, confinement, and interference) of the TMD EP have been addressed only very recently with near-field imaging where their wavelike behavior has been unraveled and characterized (*5*, *6*). These groundbreaking experiments shed light on the steady state of the EP; however, wave propagation characteristics such as group velocity can only be inferred from these dispersion measurements, and the critical transient behavior of the EP modes has remained unaddressed to date.

In parallel, in the past decade, much progress has been achieved in deep subwavelength imaging using labeled techniques such as photoactivated localization microscopy, stimulated emission depletion, and stochastic optical reconstruction microscopy (*17*–*19*), yet label-free optical microscopy remains plagued by the diffraction limit and therefore is unable to resolve details on the nanometer scale. While the scanning near-field optical microscope (SNOM) breaks this barrier, achieving up to three orders of magnitude higher resolution than conventional microscopy in the optical regime, it fails to provide extreme temporal resolution. Previous reports of near-field pump-probe spectroscopy either were based on aperture SNOM with spatial resolution limited to >100 nm or have used ultrafast sources with probe with temporal width ranging from 10 fs to 5 ps (*20*–*26*). Although these approaches have been able to probe dynamics in plasmonic systems with 10-fs resolution (*26*), to date, no report exists on time-resolved near-field imaging of photoinduced carrier dynamics in vdW materials (*27*) at extreme spatiotemporal resolution. Here, we report the direct spatiotemporal visualization of the propagation of a guided EP wave in WSe_2 slabs in the VIS-NIR spectral region and at room temperature with an unprecedented spatiotemporal resolution of 50 nm and sub–45 fs. Our novel ultrafast broadband near-field apparatus (*28*, *29*) overcomes the aforementioned limitations and enables the observation of a notably slowed down EP wave packet with a group velocity of $v_g \sim 0.017c$ in an unstructured vdW material. This observation constitutes, to the best of our knowledge, the first direct observation at the nanoscale in a TMD of the modification of the dielectric function (also known as "renormalization") introduced by an intense laser excitation around the exciton resonance (*30*). These results show that EP-supporting TMDs are a promising platform for compact slow light devices in the visible spectral range. Furthermore, our imaging technique opens up possibilities for in situ

[1]School of Physics and Astronomy, Faculty of Exact Sciences, Tel Aviv University, Tel Aviv 69978, Israel. [2]Center for Light-Matter Interaction, Faculty of Exact Sciences, Tel Aviv University, Tel Aviv 69978, Israel.
*Corresponding author. Email: haimsu@post.tau.ac.il

ultrafast coherent control in other polaritonic vdW materials and extreme spatiotemporal imaging of condensed matter systems.

RESULTS

To probe the spatiotemporal behavior of the EP formation, we have fabricated WSe_2 micrometer-scale slabs with thicknesses ranging from atomic monolayer to several tens of monolayers (see Supplementary Materials and Methods for fabrication). These slabs are characterized by two pronounced excitonic resonances A and B at 1.67 and 2.18 eV, respectively (Fig. 1A, inset). We have used a unique probe-probe near-field microscope where an apertureless SNOM has been combined with an ultrafast Ti:sapphire laser (sub–10 fs) spanning a spectrum from 650 to 1050 nm as seen in Fig. 1A. The laser beam was split into the pump, on one hand, from 650 to 700 nm and the probe, on the other hand, from 700 to 1050 nm, encompassing the A exciton transition. The probe was substantially attenuated and delayed with respect to the pump using a delay line, and the recombined beams were focused on the SNOM tip (for more details regarding the pump-probe synchronization, see the Supplementary Materials). WSe_2 slabs are scanned under the tip, which bridges the momentum gap necessary for the launching of EP by strongly localizing the incoming electrical field (Fig. 1B) (*1*, *2*). We first conducted probe-only scans to spectrally resolve the steady-state response of the flake and observed an enhanced near-field signal at 760 nm (with 10-nm bandwidth), in the vicinity of the A transition (Fig. 1C). The SNOM image clearly exhibits the interference fringes characteristic of the EP wave interacting with the incoming and outgoing light and is in agreement with recent reports (*5*, *6*) and with the calculated band diagram (see the Supplementary Materials). We then carried out pump-probe experiments and chose to probe the system at this wavelength for optimal response. In the pump-probe experiments, the probe is delayed with respect to the pump by using a precisely controlled delay line (by steps of 10 μm, $\Delta\tau \sim 66 \pm 3.3$ fs, and a total time span of 1.1 ps), and for each delay, the

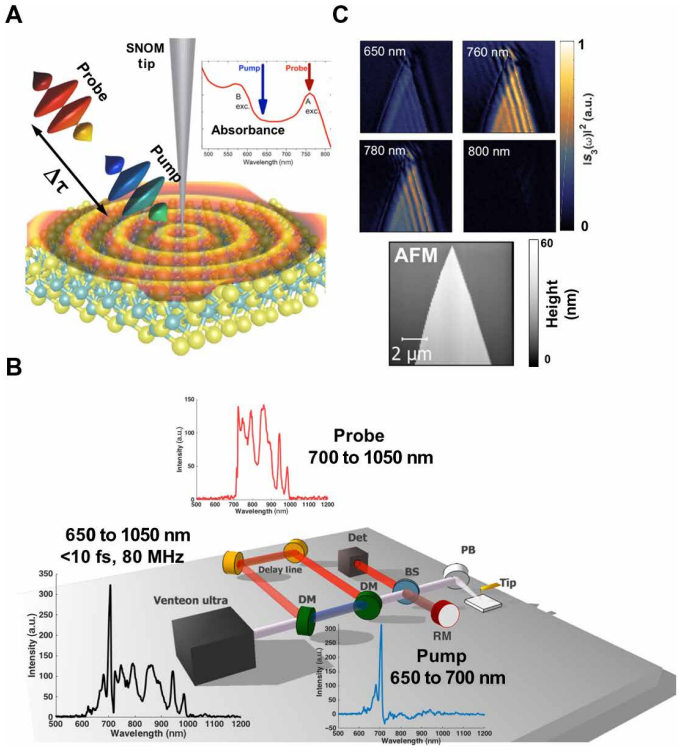

Fig. 1. Near-field ultrafast and broadband pump-probe of EP in WSe_2. (**A**) Schematic of the ultrafast pump-probe EP excitation and detection. The pump pulse impinges on the tip apex, which localizes the pulse energy, and excites an EP wave packet, which propagates on the WSe_2 slab. The wave packet is reflected at the boundaries and within the thickness of the flake and is ultimately scattered back by the tip. (**B**) Schematic of the experimental near-field pump-probe apparatus. The ultrafast sub–10-fs pulse Ti:sapphire source, spanning a broad spectrum of 650 to 1050 nm, is split by a dichroic mirror (DM) into two pulses: the pump encompassing the higher energies of 650 to 700 nm and the probe from 700 to 1050 nm. The probe is delayed with respect to the pump by steps of 66 ± 3.3 fs. The two pulses are recombined after the delay and focused onto a scattering SNOM tip. The tip is scanned across the WSe_2 slab while maintained in the vicinity of the sample's surface with a closed-loop feedback based on a tapping mode operation. Det, detector; PB, parabolic mirror; BS, 90/10 beamsplitter; RM, reference mirror; a.u., arbitrary units. (**C**) Spectrally resolved steady-state (probe only) SNOM imaging of a 60-nm-thick WSe_2 slab at several wavelengths around the exciton A bandgap. The signals are normalized with respect to the background on the SiO_2 far from the flake. We reveal an enhanced response at 760 nm, around the exciton A transition. AFM, atomic force microscopy.

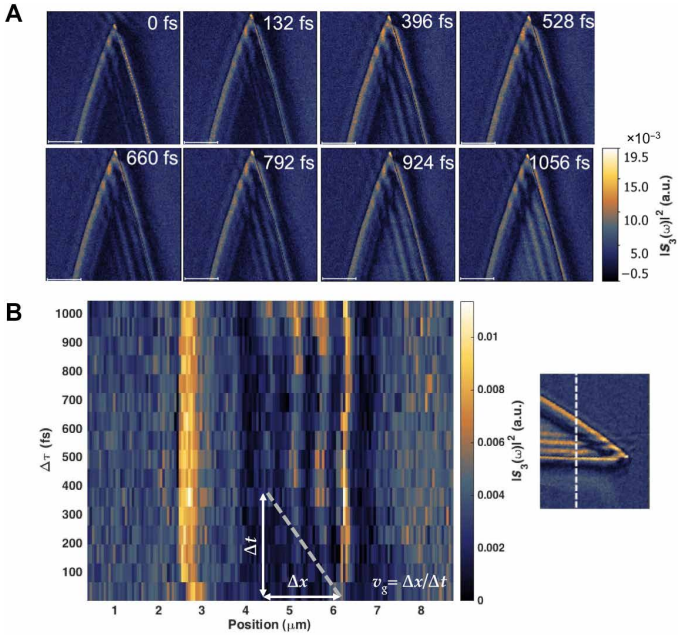

Fig. 2. Pump-probe near-field images showing the evolution of the EP wave packet in WSe_2. (**A**) Selected snapshots of the SNOM images collected at different time delays for a probe wavelength of 760 ± 5 nm. The SNOM signal depicted is $|S_3(\omega)|^2$, the intensity of the scattered signal demodulated at the third harmonic of the tip resonance frequency ω. A clear emergence of the interference fringes is observed across the flake as a function of the time delay. The thickness of the WSe_2 flake is measured to be 60 nm (~100 layers); discussion and SNOM data for flakes ranging from monolayer to more than 90 nm can be found in the main text and in the Supplementary Materials. White scale bars, 2 μm. (**B**) Two-dimensional (2D) map of the SNOM signal as a function of the position across the flake along the white dashed line (right inset) and as a function of the pump-probe time delay. We observe the consecutive appearance of interference fringes as the position goes inward inside the flake and as the time delay increases. As we show further in this article, this is the expression of the EP wave packet excited by the tip that propagates and bounces back from the nearby flakes' boundaries at a group velocity of v_g. Therefore, v_g can be retrieved by analyzing the time elapsed until the appearance of a particular fringe with respect to its position relative to the boundary. The gray dashed line is a guide for the eye to show the experimental retrieval of v_g, which we found to be equal to $4.7 \pm 0.5 \times 10^6$ m/s.

flakes are scanned under the SNOM tip covering areas of 8 μm by 8 μm with a pixel size of 50 nm. However, we note that the spatial resolution is ultimately determined by the tip size, about 50 nm, and that the temporal resolution is determined by the convolution between the pump and the probe, about 43 fs. In Fig. 2A, we present a selection of the time near-field snapshots collected (all the frames collected with a temporal step of 66 fs are supplied in the Supplementary Materials).

These time snapshots distinctly reveal a dynamical change across the slab with the emergence of the typical interference fringes over the time span of the measurements. Qualitative visualization of this change is obtained by plotting the near-field scattered signal along a cross section of the flake (depicted as the dashed white line in the inset of Fig. 2B) versus the time delay between the pump and the probe. The temporal appearance of the interference fringes is notable, and we observe their consecutive appearance with an unprecedented spatiotemporal resolution of 50 nm and sub–45 fs, first close to the flake's boundaries and then as they move inward.

To gain an understanding of the underlying physical mechanisms and as an extension of recent reports (*1*, *5*, *6*), we modeled the EP time-dependent excitation, propagation, and detection, taking into account the different contributions at different time delays to the collected signal depicted in Fig. 3A. The incoming wave is first scattered back to the detector by the tip ($E^{(0)}_{scat}$ in Fig. 3A). At the same time, it excites, via the tip, the EP mode that is guided by the flake slab-like waveguide and is back-reflected toward the tip by the nearby boundaries. Those reflections, once reaching the tip, are scattered toward the detector. Last, the light trapped in the thickness of the slab also contributes to the overall scattered signal as it exits the slab. All these contributed amplitudes add up with their respective phases at the detector and give rise to the interference patterns that we observe (Fig. 3B).

The results of our time-dependent model presented in Fig. 3B reveals that the pattern we observe are constructive interferences of the EP wave packets that propagate inside the WSe_2 slab waveguide. Therefore, this direct spatiotemporal imaging of the EP wave packet propagation allows us to retrieve its group velocity, yielding a remarkably low velocity of $v_g = 5.2 \pm 0.5 \times 10^6$ m/s, two orders of magnitude slower than the speed of light in vacuum. Such unexpectedly slow group velocity has been observed in bulk semiconductors (*31*) as a result of the renormalization 2 to 3 meV away from an exciton transition caused by exciton-light field coupling (*32*). As we show in the Supplementary Materials, the fact that such a slow group velocity is observed, in our case, as far as 40 meV away from the A exciton transition, is a clear manifestation of the growingly strong Coulomb interaction in TMD-layered materials as they thin down (*33*). In addition, from this numerical model, we have been able to retrieve the loss experienced by the EP wave and found it to be approximately $\gamma \sim 2.6\ \mu m^{-1}$, suggesting a propagation damping originating in the collision of the EP with photoinjected free electrons. These direct measurements of the EP spatiotemporal dynamics with extreme resolution therefore constitute, to the best of our knowledge, a first of its kind.

We further conducted measurements on various slab geometries, illumination, and collection configurations (see the Supplementary Materials). We found that these fringes do originate from polaritonic

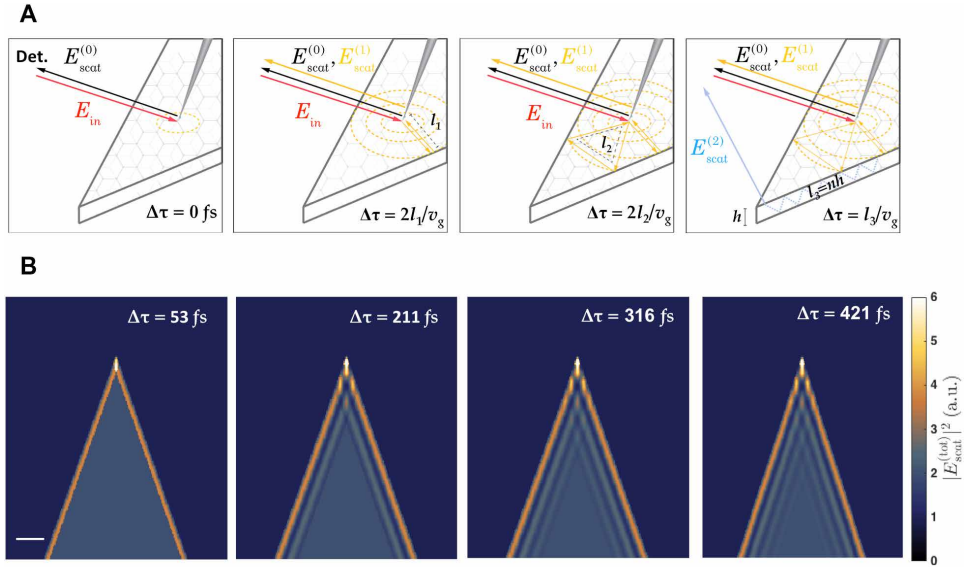

Fig. 3. Modeling of the near-field EP spatiotemporal propagation. (**A**) Schematic of the different optical paths that contribute to the SNOM signal at different time delays according to the velocity of the wave packet excited at the tip location. At $t = 0$, the EP wave packet (depicted as yellow dotted circles) is launched at the tip by the incoming field E_{in} and starts to propagate along the flake. At this point, only direct scattering by the tip $E^{(0)}_{scat}$ contributes to the near-field signal collected at the detector (Det.). Further on, as the EP wave packet propagates along the flake, it bounces back from a nearby boundary toward the tip and, at the adequate time delay that corresponds to the round trip from the tip to the boundary ($2l_1$), reaches it and contributes an additional component, $E^{(1)}_{scat}$, to the scattered near-field amplitude. Further secondary (third panel) and tertiary (not depicted) back reflections are also taken into account in accordance with previous models. An additional contribution, $E^{(2)}_{scat}$, accounts for the light trapped in the thickness of the flake and that bounces back and forth n times until it exits the flake toward the detector (depicted as a light cyan dotted line in the last panel). All these contributions add up with different phases and at different times, if at all, according to the time delay and the relative position of the tip and the flakes' boundaries. (**B**) Numerical results of the described model depicted as the total near-field scattered intensity. We observe that the model predicts the consecutive appearance of one to four fringes in about 420 fs corresponding to a group velocity of v_g ($\lambda = 760$ nm) $= 5.2 \pm 0.5 \times 10^6$ m/s, in good quantitative agreement with the experimentally retrieved v_g. Furthermore, this quantitative agreement yields a propagation loss of $\gamma \sim 2.6\ \mu m^{-1}$. This relatively high loss figure suggests that the pump pulse heavily dopes the WSe_2, causing damping of the EP via scattering with optically injected electrons. White scale bar, 1 μm.

wave packets, in agreement with dispersion calculations of the multilayer stack geometry (see the Supplementary Materials). These waves are back-reflected toward the tip by the boundaries, and therefore, their appearance strongly relies on the geometry of the flakes and the relative position of the tip to the flake's boundaries. Moreover, the asymmetry observed in the measured fringes originates from the asymmetric excitation, collection, and detection dictated by our apparatus geometry (see the Supplementary Materials). Therefore, such geometrical considerations have crucial importance in designing future devices on the basis of vdW and heterostructure materials. We also note that several experiments have been performed on single-layer and few-layered flakes and did not show such interference fringes or evolution, which support the claim that such evolution is related to the propagation mode of such materials.

DISCUSSION

We emphasize that compared to slow light schemes in atomic systems (*33*–*36*) or in periodic dielectric structures (*36*–*42*), which require bulk-material resonances, disorder, or periodic structuring, nanoscale guiding structures in two-dimensional (2D) materials inherently feature slow waves mediated by surface plasmon polaritons in graphene or surface phonon polaritons in hexagonal boron nitride. Beyond their ability to confine light beyond the diffraction limit, such platforms present the advantage of allowing the control of the speed of the guided waves via electrical doping. However, the aforementioned 2D material platforms span the mid-IR spectral region, therefore precluding their use for slow light in the VIS-NIR region. Our observations, therefore, point toward a slow light 2D platform in this important spectral region from a technological and application point of view.

In conclusion, we have reported a unique ultrafast intrapulse pump-probe near-field technique that allows one to directly visualize and quantify the EP time evolution with a spatiotemporal resolution of sub–45 fs and 50 nm in the VIS-NIR spectral region. Our technique has allowed the direct imaging of the formation and propagation of EP in WSe_2 waveguides at room temperature. We report the observation of a notably slow EP wave packet group velocity of $v_g \sim 0.017c$, two orders of magnitude slower than the speed of light. This remarkable slowing down of the group velocity originates in dispersion renormalization around the A exciton resonance. We have also found good agreement between our experimental observation and our time-dependent model that includes the contributions from both the waveguide mode and the slab geometry. Our findings suggest that vdW-based materials could be used not only as a platform for valleytronics but also for slow light with applications in light storage for memory, enhanced optical nonlinearity and sensing, and more. Last, our experimental approach opens the way for extreme spatiotemporal imaging and control of light-matter interaction.

MATERIALS AND METHODS

Preparation of WSe_2 flakes

The TMD materials of the type MX_2 (M = Mo and W; X = S and Se) consist of the hexagonal layer of metal atoms sandwiched between two layers of chalcogenide atoms. There is strong covalent bonding in the hexagonal layer and weak vdW interaction between the adjacent layers. These materials provided the evidence for high field-effect mobility and luminescence (*1*–*3*). These intensively studied layered materials have A and B exciton transitions in the visible light range. A and B excitons arise from the interlayer interactions and spin-orbit splitting (*4*), and the magnitude of the A-B splitting is independent of the number of layers (*5*). Because of their sizable bandgaps, strongly bound excitons, and high oscillator strength, these materials are expected to sustain stable polaritons at ambient conditions and thus become suitable for technological applications (*1*, *6*, *7*). Specifically, WSe_2 can be used for photovoltaic application in the conversion of solar energy into electricity because of its high absorption coefficient in the VIS-NIR spectral region and excellent output stability as photoelectrodes (*8*–*11*).

Here, the commercially available WSe_2 was mechanically exfoliated using scotch tape–based mechanical cleavage to obtain thin, highly crystalline slabs. The procedure of exfoliation was reported to be the most efficient for many 2D materials and described in detail in (*12*–*15*, *43*). Owing to the lack of control, the resulting flakes are of different shapes and thicknesses (from a few micrometers to monolayer). To enable the direct investigation of their optical properties, the WSe_2 slabs were placed on a clean surface of a 90-nm SiO_2/Si wafer. Markers were patterned by electron beam lithography and metallized with 3 nm/50 nm Ti/Au. Below, we show a typical flake under an optical microscope (with the SNOM tip) on the side.

SUPPLEMENTARY MATERIALS

Supplementary material for this article is available at http://advances.sciencemag.org/cgi/content/full/5/2/eaat9618/DC1

Fig. S1. Typical WSe_2 flake under the optical microscope with the SNOM tip.
Fig. S2. Pump and probe synchronization.
Fig. S3. Illumination geometry in our SNOM setup.
Fig. S4. Guided modes as a function of relative position between the flake and the incoming beam and polarization.
Fig. S5. SNOM images and line profile (at 3 Ω) under different illumination and collection conditions relative to the slab apex.
Fig. S6. SNOM snapshots at different time delays.
Fig. S7. Calculated dispersion [$E(k)$] map for the multilayer stack with 60-nm-thick WSe_2.
Fig. S8. Extended view of the calculated dispersion [$E(k)$] map.
Fig. S9. Dispersion curve for an EP.
Fig. S10. Group velocity of EP in WSe_2 around the A exciton transition for different longitudinal-transverse splitting.
References (*44*, *45*)

REFERENCES AND NOTES

1. D. N. Basov, M. M. Fogler, F. J. Garcia de Abajo, Polaritons in van der Waals materials. *Science* **354**, aag1992 (2016).
2. T. Low, A. Chaves, J. D. Caldwell, A. Kumar, N. X. Fang, P. Avouris, T. F. Heinz, F. Guinea, L. Martin-Moreno, F. Koppens, Polaritons in layered two-dimensional materials. *Nat. Mater.* **16**, 182–194 (2017).
3. J. A. Wilson, A. D. Yoffe, The transition metal dichalcogenides discussion and interpretation of the observed optical, electrical and structural properties. *Adv. Phys.* **18**, 193–335 (1969).
4. Q. Wang, L. Sun, B. Zhang, C. Chen, X. Shen, W. Lu, Direct observation of strong light-exciton coupling in thin WS_2 flakes. *Opt. Express* **24**, 7151–7157 (2016).
5. F. Hu, Y. Luan, M. E. Scott, J. Yan, D. G. Mandrus, X. Xu, Z. Fei, Imaging exciton–polariton transport in $MoSe_2$ waveguides. *Nat. Photonics* **11**, 356–360 (2017).
6. Z. Fei, M. E. Scott, D. J. Gosztola, J. J. Foley IV, J. Yan, D. G. Mandrus, H. Wen, P. Zhou, D. W. Zhang, Y. Sun, J. R. Guest, S. K. Gray, W. Bao, G. P. Wiederrecht, X. Xu, Nano-optical imaging ofWSe_2 waveguide modes revealing light-exciton interactions. *Phys. Rev. B* **94**, 081402 (2016).
7. F. Keilmann, R. Hillenbrand, A. Zayats, D. Richard, *Near-Field Nanoscopy by Elastic Light Scattering from a Tip* (Artech House Norwood, 2009).
8. R. Hillenbrand, F. Keilmann, Complex optical constants on a subwavelength scale. *Phys. Rev. Lett.* **85**, 3029–3032 (2000).
9. S. Dai, Q. Ma, M. K. Liu, T. Andersen, Z. Fei, M. D. Goldflam, M. Wagner, K. Watanabe, T. Taniguchi, M. Thiemens, F. Keilmann, G. C. A. M. Janssen, S.-E. Zhu, P. Jarillo-Herrero, M. M. Fogler, D. N. Basov, Graphene on hexagonal boron nitride as a tunable hyperbolic metamaterial. *Nat. Nanotechnol.* **10**, 682–686 (2015).

10. S. Dai, Z. Fei, Q. Ma, A. S. Rodin, M. Wagner, A. S. McLeod, M. K. Liu, W. Gannett, W. Regan, K. Watanabe, T. Taniguchi, M. Thiemens, G. Dominguez, A. H. C. Neto, A. Zettl, F. Keilmann, P. Jarillo-Herrero, M. M. Fogler, D. N. Basov, Tunable phonon polaritons in atomically thin van der Waals crystals of boron nitride. *Science* **343**, 1125–1129 (2014).
11. A. Woessner, M. B. Lundeberg, Y. Gao, A. Principi, P. Alonso-González, M. Carrega, K. Watanabe, T. Taniguchi, G. Vignale, M. Polini, J. Hone, R. Hillenbrand, F. H. L. Koppens, Highly confined low-loss plasmons in graphene–boron nitride heterostructures. *Nat. Mater.* **14**, 421–425 (2015).
12. Z. Fei, A. S. Rodin, G. O. Andreev, W. Bao, A. S. McLeod, M. Wagner, L. M. Zhang, Z. Zhao, M. Thiemens, G. Dominguez, M. M. Fogler, A. H. C. Neto, C. N. Lau, F. Keilmann, D. N. Basov, Gate-tuning of graphene plasmons revealed by infrared nano-imaging. *Nature* **487**, 82–85 (2012).
13. J. A. Gerber, S. Berweger, B. T. O'Callahan, M. B. Raschke, Phase-resolved surface plasmon interferometry of graphene. *Phys. Rev. Lett.* **113**, 055502 (2014).
14. A. Beal, W. Y. Liang, Excitons in 2H-WSe_2 and 3R-WS_2. *J. Phys. C Solid State Phys.* **9**, 2459 (1976).
15. L. C. Flatten, Z. He, D. M. Coles, A. A. P. Trichet, A. W. Powell, R. A. Taylor, J. H. Warner, J. M. Smith, Room-temperature exciton-polaritons with two-dimensional WS_2. *Sci. Rep.* **6**, 33134 (2016).
16. X. Liu, T. Galfsky, Z. Sun, F. Xia, E.-c. Lin, Y.-H. Lee, S. Kéna-Cohen, V. M. Menon, Strong light–matter coupling in two-dimensional atomic crystals. *Nat. Photonics* **9**, 30–34 (2015).
17. E. Betzig, G. H. Patterson, R. Sougrat, O. W. Lindwasser, S. Olenych, J. S. Bonifacino, M. W. Davidson, J. Lippincott-Schwartz, H. F. Hess, Imaging intracellular fluorescent proteins at nanometer resolution. *Science* **313**, 1642–1645 (2006).
18. T. A. Klar, S. Jakobs, M. Dyba, A. Egner, S. W. Hell, Fluorescence microscopy with diffraction resolution barrier broken by stimulated emission. *Proc. Natl. Acad. Sci. U.S.A.* **97**, 8206–8210 (2000).
19. S. J. Sahl, W. E. Moerner, Super-resolution fluorescence imaging with single molecules. *Curr. Opin. Struct. Biol.* **23**, 778–787 (2013).
20. E. Yoxall, M. Schnell, A. Y. Nikitin, O. Txoperena, A. Woessner, M. B. Lundeberg, F. Casanova, L. E. Hueso, F. H. L. Koppens, R. Hillenbrand, Direct observation of ultraslow hyperbolic polariton propagation with negative phase velocity. *Nat. Photonics* **9**, 674–678 (2015).
21. H. Haug, R. März, S. Schmitt-Rink, Dielectric function for semiconductors with a high exciton concentration. *Phys. Lett. A* **77**, 287–288 (1980).
22. T. Virgili, G. Grancini, E. Molotokaite, I. Suarez-Lopez, S. K. Rajendran, A. Liscio, V. Palermo, G. Lanzani, D. Polli, G. Cerullo, Confocal ultrafast pump–probe spectroscopy: A new technique to explore nanoscale composites. *Nanoscale* **4**, 2219–2226 (2012).
23. M. Wagner, Z. Fei, A. S. McLeod, A. S. Rodin, W. Bao, E. G. Iwinski, Z. Zhao, M. Goldflam, M. Liu, G. Dominguez, M. Thiemens, M. M. Fogler, A. H. Castro Neto, C. N. Lau, S. Amarie, F. Keilmann, D. N. Basov, Ultrafast and nanoscale plasmonic phenomena in exfoliated graphene revealed by infrared pump–probe nanoscopy. *Nano Lett.* **14**, 894–900 (2014).
24. S. A. Dönges, O. Khatib, B. T. O'Callahan, J. M. Atkin, J. H. Park, D. Cobden, M. B. Raschke, Ultrafast nanoimaging of the photoinduced phase transition dynamics in VO_2. *Nano Lett.* **16**, 3029–3035 (2016).
25. G. X. Ni, L. Wang, M. D. Goldflam, M. Wagner, Z. Fei, A. S. McLeod, M. K. Liu, F. Keilmann, B. Özyilmaz, A. H. Castro Neto, J. Hone, M. M. Fogler, D. N. Basov, Ultrafast optical switching of infrared plasmon polaritons in high-mobility graphene. *Nat. Photonics* **10**, 244–247 (2016).
26. V. Kravtsov, R. Ulbricht, J. M. Atkin, M. B. Raschke, Plasmonic nanofocused four-wave mixing for femtosecond near-field imaging. *Nat. Nanotechnol.* **11**, 459–464 (2016).
27. P. Steinleitner, P. Merkl, P. Nagler, J. Mornhinweg, C. Schüller, T. Korn, A. Chernikov, R. Huber, Direct observation of ultrafast exciton formation in a monolayer of WSe_2. *Nano Lett.* **17**, 1455–1460 (2017).
28. M. Mrejen, L. Yadgarov, A. Levanon, H. Suchowski, Ultrafast near-field dynamics of polariton-exciton in WSe_2 slab waveguides at room temperature, in *Conference on Lasers and Electro-Optics*, paper FM2F.5 (Optical Society of America, 2018).
29. M. Mrejen, L. Yadgarov, A. Levanon, H. Suchowski, Ultrafast near-field dynamics of exciton-polariton in WSe_2 at room temperature, in *Advanced Photonics 2018*, paper NoW4J.1 (Optical Society of America, 2018).
30. K. Kempf, G. Schmieder, G. Kurtze, C. Klingshirn, Excitation induced renormalization effects of the excitonic polariton dispersion in CdS. *Phys. Stat. Sol. B* **107**, 297–306 (1981).
31. R. G. Ulbrich, G. W. Fehrenbach, Polariton wave packet propagation in the exciton resonance of a semiconductor. *Phys. Rev. Lett.* **43**, 963–966 (1979).
32. J. J. Hopfield, Resonant scattering of polaritons as composite particles. *Phys. Rev.* **182**, 945–925 (1969).
33. H. Yu, X. Cui, X. Xu, W. Yao, Valley excitons in two-dimensional semiconductors. *Natl. Sci. Rev.* **2**, 57–70 (2015).
34. L. V. Hau, S. E. Harris, Z. Dutton, C. H. Behroozi, Light speed reduction to 17 metres per second in an ultracold atomic gas. *Nature* **397**, 594–598 (1999).
35. L. Novotny, B. Hecht, *Principles of Nano-Optics* (Cambridge Univ. Press, 2012).
36. M. D. Lukin, A. Imamoğlu, Controlling photons using electromagnetically induced transparency. *Nature* **413**, 273–276 (2001).
37. K. L. Tsakmakidis, O. Hess, R. W. Boyd, X. Zhang, Ultraslow waves on the nanoscale. *Science* **358**, eaan5196 (2017).
38. T. Baba, Slow light in photonic crystals. *Nat. Photonics* **2**, 465–473 (2008).
39. Y. A. Vlasov, M. O'boyle, H. F. Hamann, S. J. McNab, Active control of slow light on a chip with photonic crystal waveguides. *Nature* **438**, 65–69 (2005).
40. A. Yariv, Y. Xu, R. K. Lee, A. Scherer, Coupled-resonator optical waveguide: A proposal and analysis. *Opt. Lett.* **24**, 711–713 (1999).
41. B. Corcoran, C. Monat, C. Grillet, D. J. Moss, B. J. Eggleton, T. P. White, L. O'Faolain, T. F. Krauss, Green light emission in silicon through slow-light enhanced third-harmonic generation in photonic-crystal waveguides. *Nat. Photonics* **3**, 206–210 (2009).
42. M. Soljačić, S. G. Johnson, S. Fan, M. Ibanescu, E. Ippen, J. D. Joannopoulos, Photonic-crystal slow-light enhancement of nonlinear phase sensitivity. *JOSA B* **19**, 2052–2059 (2002).
43. N. Lundt, S. Klembt, E. Cherotchenko, S. Betzold, O. Iff, A. V. Nalitov, M. Klaas, C. P. Dietrich, A. V. Kavokin, S. Höfling, C. Schneider, Room-temperature Tamm-plasmon exciton-polaritons with a WSe_2 monolayer. *Nat. Commun.* **7**, 13328 (2016).
44. X. Liu, W. Bao, Q. Li, C. Ropp, Y. Wang, X. Zhang, Control of coherently coupled exciton polaritons in monolayer tungsten disulphide. *Phys. Rev. Lett.* **119**, 027403 (2017).
45. A. J. Sternbach, J. Hinton, T. Slusar, A. S. McLeod, M. K. Liu, A. Frenzel, M. Wagner, R. Iraheta, F. Keilmann, A. Leitenstorfer, M. Fogler, H.-T. Kim, R. D. Averitt, D. N. Basov, Artifact free time resolved near-field spectroscopy. *Opt. Express* **25**, 28589–28611 (2017).

Acknowledgments: We acknowledge D. Naveh (Bar-Ilan University, Israel) for providing help and for the synthesis of the WSe_2 flakes. **Funding:** This research was supported by the European Research Council (ERC), under the project MIRAGE 20-15 and H2020 grant no. 639402, and the Israel Science Foundation (ISF), under grant no. 1433/15. **Author contributions:** L.Y. fabricated the samples. M.M. and L.Y. performed the SNOM scans. M.M. and L.Y. analyzed the data. M.M. and A.L. developed the ultrafast near-field apparatus. M.M. developed the model. H.S. supervised the research. All authors contributed to writing the manuscript. **Competing interests:** The authors declare that they have no competing interests. **Data and materials availability:** All data needed to evaluate the conclusions in the paper are present in the paper and/or the Supplementary Materials. Additional data related to this paper may be requested from the authors.

Submitted 23 April 2018
Accepted 17 December 2018
Published 1 February 2019
10.1126/sciadv.aat9618

Citation: M. Mrejen, L. Yadgarov, A. Levanon, H. Suchowski, Transient exciton-polariton dynamics in WSe_2 by ultrafast near-field imaging. *Sci. Adv.* **5**, eaat9618 (2019).

Science Advances

Transient exciton-polariton dynamics in WSe_2 by ultrafast near-field imaging

M. Mrejen, L. Yadgarov, A. Levanon and H. Suchowski

Sci Adv **5** (2), eaat9618.
DOI: 10.1126/sciadv.aat9618